Phase transition in twinned nanolayered silicon structures under uniaxial compression: Molecular dynamics simulations and first-principles total-energy calculations

V. I. Ivashchenko[1] and P. E. A. Turchi[2]
[1]*Institute of Problems of Materials Science, NAS of Ukraine, Krzhyzhanovsky str. 3, 03142 Kyiv, Ukraine*
[2]*Lawrence Livermore National Laboratory (L-352), P.O. Box 808, Livermore, California 94551, USA*
(Received 18 March 2010; revised manuscript received 29 April 2010; published 20 May 2010)

Molecular dynamics simulations and first-principles total-energy calculations were carried out to investigate the behavior of nanolayered (111) twinned silicon structures under uniaxial compression. The diamondlike silicon structure inside the thin (<3 nm) twin layers was found to transform to the orthorhombic structure (space group *Fmmm*) at ~25 GPa under uniaxial compression and to the tetragonal structure (space group $I4/mmm$) upon decompression. The first structural transformation is a first-order phase transition and the new structure is characterized by an increased failure stress above 37 GPa. First-principles pseudopotential calculations confirmed the formation of the tetragonal phase and showed that both the orthorhombic and tetragonal phases would possess metal properties.

DOI: 10.1103/PhysRevB.81.195213 PACS number(s): 61.50.Ks, 61.72.uf, 64.75.Jk, 71.20.Mq

I. INTRODUCTION

Silicon exhibits a set of structural transformations under hydrostatic pressure.[1] In particular, bulk silicon crystalline-silicon (c-Si) (diamondlike phase with space group $Fd\bar{3}m$) undergoes the following phase transformations under compression and upon decompression: The c-Si structure transforms to the tetragonal body-centered metallic β-tin (β-Si) phase ($I4_1/amd$) at ~11–12.5 GPa.[1,2] The β-Si phase undergoes a transformation to the related *Imma* structure at 13 GPa.[3,4] A further increase in pressure leads to the appearance of a simple hexagonal (sh) ($P6_3/mmc$) structure near 16 GPa.[2–5] At pressures above 40 GPa and 80 GPa, the hexagonal-closed-packed and the face-centered-cubic structure are observed, respectively.[1] Bulk Si does not transform back to the ground-state c-Si structure upon full pressure release. Instead, a variety of metastable crystalline and amorphous phases have been reported.[6,7] Among them, the cubic body centered bc8 ($Ia\bar{3}$), tetragonal st12 ($P4_222$), and rhombohedral r8 ($R\bar{3}$) structures are observed.[6,8,9] Amorphous semiconductor silicon transforms to the metallic amorphous high-density phase at approximately 10 GPa.[10] Most of the observed phase transitions in c-Si under hydrostatic pressure were successfully accounted for in the framework of various empirical potential and first-principles approaches.[11–15]

The effect of uniaxial strain on silicon structures was investigated to a smaller extent. To the best of our knowledge, there are only a few first-principles investigations devoted to this problem.[16,17] Stable phases under uniaxial compression were found to be c-Si, β-Si, and sh structures, i.e., the same as those observed under hydrostatic condition.[16] At high uniaxial compressions of Si nanospheres, the creation of β-Si in the particle core led to volumetric changes, an increase in elastic moduli, and significant hardening.[17]

Recently, using the fact that Si layers grown epitaxial on a *B*-induced Si (111) $\sqrt{3}\times\sqrt{3}$ surface have a twinned orientation with respect to the substrate,[18] the Si twinning superlattices have been grown by molecular-beam epitaxy.[19,20] Highly boron-doped Si(111) samples were used as substrates. The $\sqrt{3}\times\sqrt{3}$ reconstruction was prepared using the surface segregation of during annealing. The thickness of the twinned layers did not exceed 2.5–3 nm.[20] So far, we did not found any study on uniaxial phase transitions in nanolayered silicon twinned structures. The investigation of the behavior of such structures under uniaxial compression could enhance our knowledge on silicon nanostructures and enable us to suggest possible fields of applications.

In this paper we report the results of the study of nanolayered twinned silicon structures under uniaxial compression. The investigations were carried out using molecular dynamics (MD) simulations based on the Tersoff potential and a first-principles pseudopotential approach. The emphasis was put on the structures that were composed of a sequence of twin segments in the (111) direction and new fivefold-coordinated orthorhombic and tetragonal silicon phases inside the twin segments were predicted.

The paper is organized as follows. In Sec. II we present our theoretical framework and the computational details. Section III contains the results of molecular dynamics simulations and first-principles calculations and their significance. Finally, Sec. IV contains the main conclusions.

II. MODELING AND COMPUTATIONAL ASPECTS

Twinned nanolayered silicon structures of 5760 atoms were represented by rectangular prisms ($4.0\times3.8\times7.5$ nm^3) that consisted of 1, 2, 4, and 8 twin nanosized segments oriented perpendicularly to the z direction. The z axis was aligned with the (1 1 1) direction of crystalline silicon. The four twinned structures, t-1, t-2, t-4, and t-8, with segment thicknesses of 7.5 nm, 3.3 nm, 1.9 nm, and 0.9 nm, respectively, were generated. The x axis and y axis in the odd segments were aligned along the $(11\bar{2})$ and $(1\bar{1}0)$ directions in c-Si, respectively, whereas in the even segments, they were aligned along the $(\bar{1}\bar{1}2)$ and $(\bar{1}10)$ directions, respectively.

Molecular dynamics simulations based on the Tersoff potential[21] were performed for these structures under uniaxial strains by using the XMD code.[22] Initial samples

were equilibrated for 10 ps at 300 K. To determine the stress-strain curves we used the following approach: at each time interval (1000 MD steps that correspond to approximately 1.0 ps), the systems were uniaxially compressed by applying a positive external pressure along the z direction, $Pz=n\Delta P$, where n is a number of time intervals and ΔP is a small pressure increment. We chose $\Delta P=0.002$ Mbar. The simulations were carried out at 300 K in the *NPT* ensemble (constant number of particles-pressure-temperature) with periodic boundary conditions, supporting the bulk modulus B constant. Since at each time interval the atomic forces relaxed, the normal and lateral dimensions were optimized. Such a procedure provides a strain rate of 10^9 s^{-1}. The z component of the atomic stress tensor was calculated and averaged over a region of space to obtain a macroscopic stress field.[22] We also used $\Delta P=0.008$ Mbar, in which case the macroscopic stress increased but the structural transformations were unaffected. During decompression, a similar approach was used. The final decompressed structures were equilibrated for 10 ps at 300 K.

Calculations of the cubic ($Fd\bar{3}m$) and tetragonal ($I4/mmm$) silicon structures were carried out using the QUANTUM-ESPRESSO first-principles code[23] for 8-atom unit cells. Vanderbilt ultrasoft pseudopotentials were used to describe the electron-ion interaction.[24] In this approach, the orbitals are allowed to be as soft as possible in the core regions so that their plane-wave expansion converges rapidly.[24] The nonlinear core corrections were taken into account.[23] To describe the exchange-correlation energy, the generalized gradient approximation[25] was employed. The criterion of convergence for the total energy was 10^{-6} Ry/f.u. To speed up convergence, each eigenvalue was convoluted with a Gaussian with a width of 0.02 Ry. The cutoff energy for the plane-wave basis was set to 32 Ry. The integration in the Brillouin zone was performed with a set of special k points determined according to the Monkhorst-Pack scheme[26] using a $(8\times8\times8)$ mesh. The densities of states (DOSs) of the cubic, orthorhombic, and tetragonal silicon structures were calculated with the tetrahedron method.[23]

The equilibrium geometry of each structure under consideration was calculated by considering the simultaneous relaxations of the ions and of the unit cells without preserving the symmetry with a Parinello-Rahman method.[27] The relaxation of the atomic coordinates and of the unit cell was considered to be complete when the atomic forces were less than 1.0 mRy/bohr, the stresses were smaller than 0.05 GPa, and the total energy during the structural optimization iterative process was changing by less than 0.1 mRy.

III. RESULTS AND DISCUSSION

A. Empirical-potential molecular dynamics simulations

The stress-strain curves of the t-1, t-2, t-4, and t-8 twin silicon structures under uniaxial compression are shown in Fig. 1. At uniaxial compression strains <0.3, all the samples exhibit usual stress-stress relations with yield and flow stresses of ~12 GPa and 25 GPa, respectively. None of the samples shows an increase in flow stress caused by nanosegmentation. However, and in contrast to the t-1 and t-2 structures, for the t-4 and t-8 samples, a further increase in strain leads to a drastic increase in stress that reaches 37 GPa. This indicates a different nature in the structural transformation for these two sets of samples under uniaxial strain.

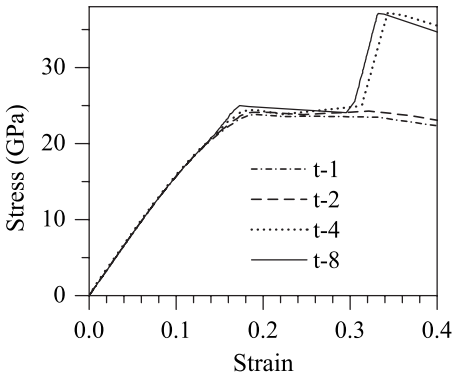

FIG. 1. Stress of the twinned structures as a function of uniaxial compression strain.

To gain insight into the mechanism that operate during the structural transformation exhibited by these twinned structures we calculated the pair-correlation function (PCF) and the bond-angle distribution $[g(\Theta)]$ of the t-1 sample under the uniaxial strain $\varepsilon=0.32$, which corresponds to the flat region in the stress-strain curve (cf. Fig. 1). In Fig. 2 we compare the calculated functions for the t-1 sample with those for the high-density amorphous (HDA) structure that was generated by hydrostatic compression of the initial low-density amorphous (LDA) silicon at 9–10 GPa.[28] Let us recall that the LDA to HDA pressure-induced phase transition at 10 GPa was first experimentally reported in Ref. 10. We see that both distributions are similar. However some discrepancies exist. Therefore, we assume that the plastic flow of the t-1 and t-2 sample caused by uniaxial compression occurs through amorphization. In the plastic-flow region, the struc-

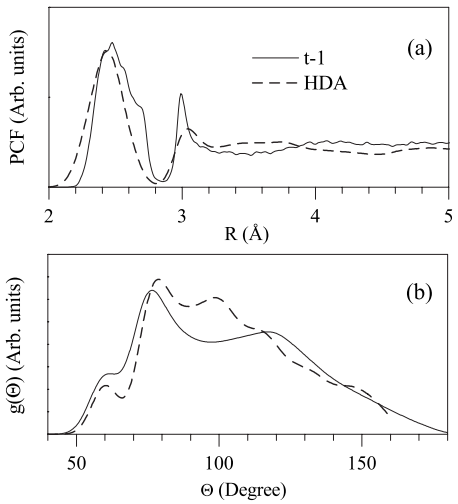

FIG. 2. PCFs and bond-angle distributions $[g(\Theta)]$ of the t-5760 structure without twin segments (t-1) and under compression strain of $\varepsilon=0.32$ (full line) and those of the HDA structure obtained in Ref. 28 (dashed line).

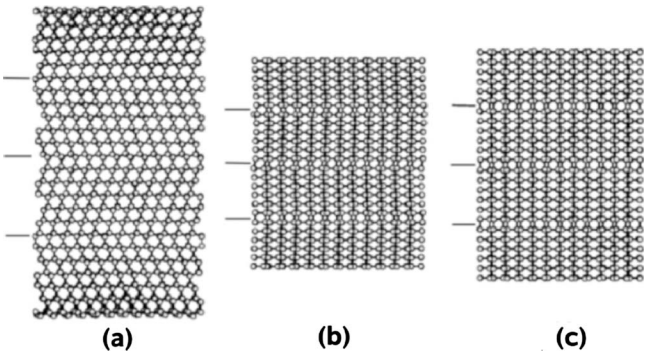

FIG. 3. Projection of the atomic configurations of the t-4 structure on the *y*-*z* plane: (a) without strain, $\varepsilon=0$; (b) under uniaxial compression with a strain $\varepsilon=0.315$; and (c) after decompression. The horizontal lines locate the interfaces between the twin segments.

ture of these samples can be considered as a mixture of HDA and compressed c-Si structures.

A quite different phenomenon is observed for the t-4 and t-8 twinned structures. In Fig. 3 we show the atomic configurations of the t-4 sample at different stages of uniaxial compression and decompression. We see that the flat region in the stress-strain curve of this sample can be assigned to the formation of a new ordered structure. Hence in this case, the phase transition is associated to the transformation from the initial twinned structure to another ordered structure. This structural transformation is a first-order phase transition that is accompanied with a volume jump, which is corroborated by the calculated dependence of the sample volume on uniaxial pressure as shown in Fig. 4.

The mechanism of formation of the new ordered structure under uniaxial compression is illustrated in Fig. 5. It is seen that, at first, uniaxial compression leads to a "flattening" of the atomic arrangement on the *x*-*y* planes that are situated parallel to the twin interfaces [cf. Fig. 5(b)]. Upon further compression, these planes shift in pairs in opposite directions in the *y* direction [cf. Fig. 5(c)]. As a result, a new fivefold-coordinated structure forms. Since the described structural transformation under uniaxial compression is not observed for the t-1 and t-2 samples, we predict that it will take place only for the (111) twinned silicon structures with segment thickness not exceeding ~3 nm. For the twinned structures under consideration, the twin interfaces are the planes of easy slip. The shift of the atomic planes initiated by uniaxial compression will begin in a parallel way to these interfaces

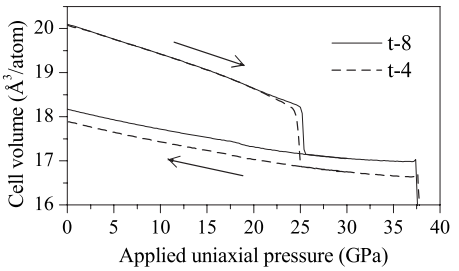

FIG. 4. Sample volume of the t-4 and t-8 structures as a function of the uniaxial pressure during compression and decompression.

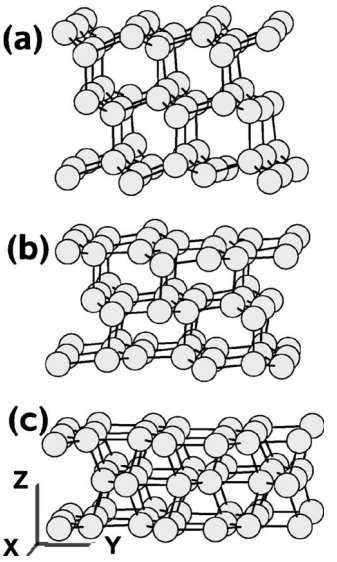

FIG. 5. Evolution of the atomic configuration of one of the segments of the t-4 structure under uniaxial compression with a strain: (a) $\varepsilon=0$, (b) $\varepsilon=0.172$, and (c) $\varepsilon=0.315$. The *x*, *y*, and *z* axes correspond to the $(11\bar{2})$, $(1,\bar{1}0)$, and (1 1 1) directions in c-Si.

in opposite directions. The thinner the twin segments are, the easier the slip of the atomic planes is. Therefore, uniaxial compression leads to the creation of the new fivefold-coordinated structure only in the twinned structures with thin segments.

During decompression, the initial structure is not recovered [cf. Figs. 3(c) and 4]: the new fivefold-coordinated structure lengthens, however, does not recover completely. Indeed, Fig. 4 shows that the volume of the decompressed structures is smaller by ~10% as compared to the one of the compressed samples.

A comprehensive analysis of the atomic configurations of the compressed and decompressed t-4 structures enabled us to identify their crystalline structures. For this purpose, the initial unit cells were built by extracting the repeated cells inside several segments and after averaging. The final crystalline structures were then identified with the help of the ISOTROPY code.[29] The compressed and decompressed t-4 structures were identified as the orthorhombic (space group

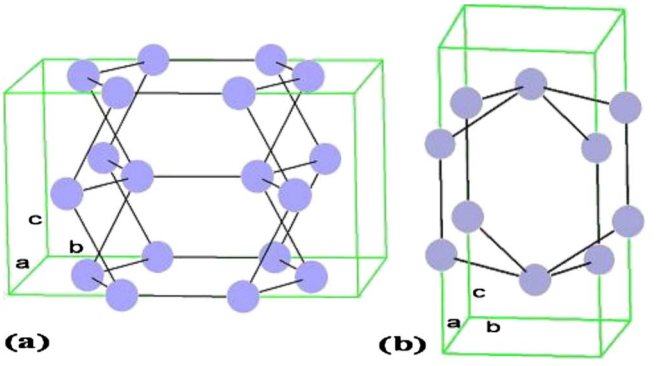

FIG. 6. (Color online) Unit cells of the primitive (a) orthorhombic (space group *Fmmm*) and (b) tetragonal (space group *I*4/*mmm*) lattices (cf. Table I).

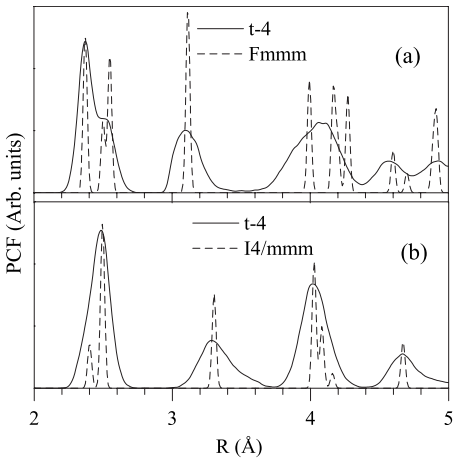

FIG. 7. PCF of the t-4 structures (solid line) (a) under compression with strain $\varepsilon=0.315$ and (b) upon decompression. [(a) and (b)] PCFs of the predicted structures (dashed line).

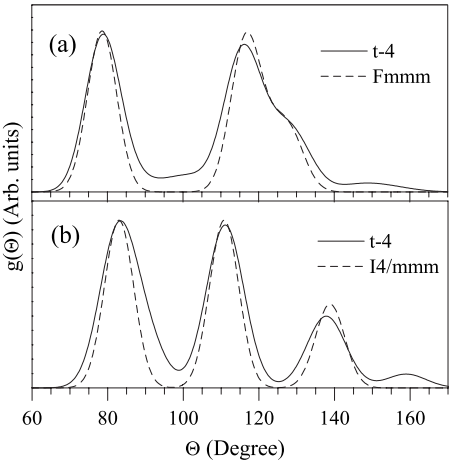

FIG. 8. Bond-angle distributions $[g(\theta)]$ of the t-4 structures (solid line) (a) under compression strains $\varepsilon=0.315$ and (b) upon decompression. [(a) and (b)] The $g(\theta)$ dependencies of the identified structures (dashed line).

Fmmm) and tetragonal (space group $I4/mmm$) structures. The primitive orthorhombic and tetragonal unit cells are shown in Fig. 6. The orthorhombic cell transforms into the tetragonal one provided $c=a$. The cell parameters of both structures are summarized in Table I. The bond lengths of the nearest five neighbors are distributed as follows: 1–2.500 Å, 2–2.371 Å, and 2–2.550 Å for the *Fmmm* phase, and 1–2.401 Å and 4–2.495 Å for the $I4/mmm$ phase. For the sake of comparison, in c-Si, the bond length is 2.351 Å.

We calculated the pair-correlation functions and bond-angle distributions for the compressed and decompressed t-4 structures as well as for the predicted *Fmmm* and $I4/mmm$ structures. The computed dependences are shown in Figs. 7 and 8. It is seen that the corresponding curves agree rather well. Some observed discrepancies are caused by the fact that the predicted *Fmmm* and $I4/mmm$ structures reflect structures inside the segments, whereas the t-4 structures include also twin interfaces.

B. First-principles calculations

The *Fmmm* to $I4/mmm$ transformation upon decompression was confirmed by the results of first-principles calculations. We optimized the *Fmmm* structure using the pseudopotential approach.[23] The structural relaxation was carried out without preservation of cell symmetry and by allowing cell variation. The final $I4/mmm$ relaxed structure is found to be close to the corresponding structure predicted from MD simulations (cf. Table I). This result validates to a large extent the empirical procedure used in the present investigation.

To draw an analogy to uniform compression, we investigated the total energy E_T and the Gibbs free energy $H=E_T+PV$ at zero temperature for the c-Si and $I4/mmm$ phases as functions of cell volume and pressure, respectively. These dependencies, calculated using first-principles and empirical procedures, are presented in Fig. 9. One can see that the total energy and the Gibbs free energy calculated with both approaches agree fairly well. In particular, the pressures of the c-Si to $I4/mmm$ transition, predicted by both methods practically coincide. We note here that the new fivefold-coordinated silicon phases could not be detected under hydrostatic pressure, since the silicon (space group $Fd\bar{3}m$) first transforms into the tetragonal β-tin polytype (space group $I4_1/amd$) at pressure in the range 11–12.5 GPa that is lower than the pressure of ~17 GPa, at which the new stable

TABLE I. Symmetry, lattice parameters (a, b, and c), atomic positions (in terms of a, b, and c), and Wyckoff positions (WPs) of the ordered structures after uniaxial compression and decompression of the t-4 structure.

Structure	Symmetry	a (Å)	b (Å)	c (Å)	WP	x	y	z
Unstrained ($\varepsilon=0$)	$Fd\bar{3}m$ (No. 227)	5.430 5.469[a]			8*b* (0 0 0)	0.625 0.375	0.625 0.375	0.625 0.375
Compressed ($\varepsilon=0.315$)	*Fmmm* (No. 69)	4.602	7.199	4.200	8*h* (0 0.674 0)	0.500 0.500	0.326 0.674	0.500 0.500
Decompressed ($\varepsilon=0.315-0.0$)	$I4/mmm$ (No. 139)	3.302 3.380[a]	3.302 3.380[a]	6.560 6.167[a]	4*e* (0 0.683 0)	0.000 0.000	0.000 0.000	0.317 0.683

[a]Present results based on first-principles pseudopotential calculation.

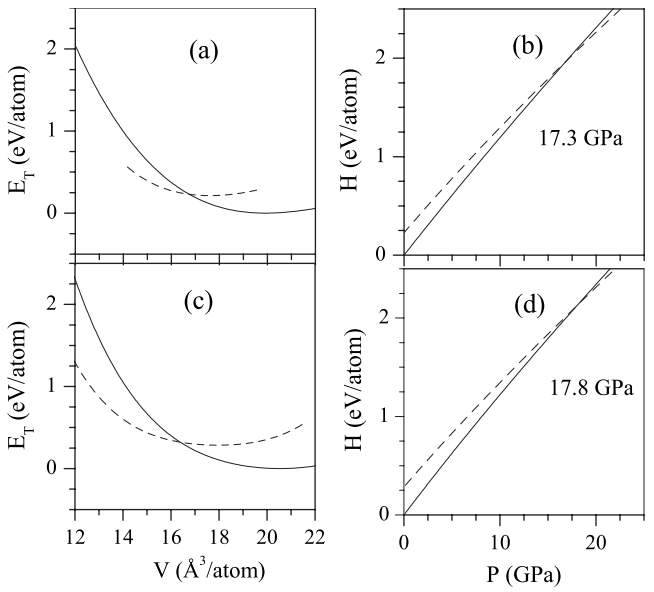

FIG. 9. Total (E_T) energy-cell volume (V) and Gibbs free energy (H), pressure (P) dependencies for the $Fd\bar{3}m$ (solid line), and $I4/mmm$ (dashed line) structures calculated by using [(a) and (b)] the Tersoff approach and [(c) and (d)] the first-principles pseudopotential method.

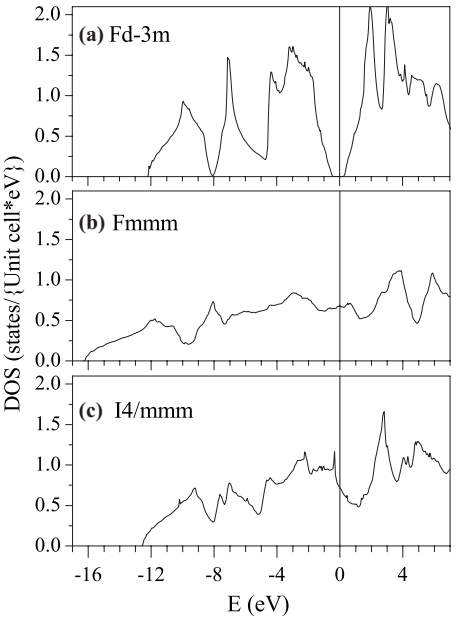

FIG. 10. DOSs of several Si structures: (a) the diamondlike phase (space group $Fd\bar{3}m$) and the model structures having space groups (b) $Fmmm$ and (c) $I4/mmm$. The DOS have been calculated with the first-principles pseudopotential method using primitive 8-atom (a) cubic, (b) orthorhombic, and (c) tetragonal unit cells, respectively. The Fermi energy is located at the zero of energy.

$I4/mmm$ phase forms. The fivefold-coordinated $I4/mmm$ silicon phases can form upon decompression of the compressed $Fmmm$ structure at room temperature. In turn, the latter phase arises provided uniaxial compression is imposed on the (111) twinned silicon structures with thin segments. Nevertheless, it is worth noting the analogy between the $Fd\bar{3}m$(c-Si)-$I4_1/amd$(β-tin)-$P4_222$(st12) transitions in bulk Si under hydrostatic compression and decompression and the $Fd\bar{3}m$-$Fmmm$-$I4/mmm$ transitions in Si twinned structures under uniaxial compression and decompression.

In Fig. 10, the total DOSs of the initial cubic silicon structure and of the phases of the t-4 structure that are stabilized under uniaxial compression and decompression are shown. The initial structure is semiconducting, whereas the orthorhombic and orthogonal phases are metallic. The cubic silicon exhibits a band gap ~1.1 eV that is higher than the value found in our calculations (~0.7 eV). This discrepancy is due to the well-known underestimation of the band gaps by density-functional theory. We see that the decompression of the orthorhombic structure leads to the formation of a distinct minimum in the DOS. Nevertheless, the decompressed tetragonal phase remains metallic. One can expect that, for the metallic phases, the high DOS at the Fermi level may give rise to superconductivity.

IV. CONCLUSIONS

Molecular dynamics simulations of nanolayered silicon twinned structures under uniaxial compression enabled us to arrive at the following conclusions: (1) uniaxial compression of the (111) twinned silicon nanolayered structures causes the formation of segmented structures with the fivefold-coordinated orthorhombic structure (space group $Fmmm$) inside these segments at ~25 GPa. Such a structural transformation only occurs for the twinned nanolayered structures with layer thickness not exceeding ~3 nm. This transformation is a first-order phase transition and the new structure is characterized by an increase in the failure stress above 37 GPa. The orthorhombic phase transforms into the tetragonal one (space group $I4/mmm$) after decompression at 300 K. (2) First-principles pseudopotential calculations confirmed the formation of the tetragonal phase predicted from empirical-potential molecular dynamics simulations and showed that both the orthorhombic and tetragonal phases will exhibit a metallic character. (3) Finally, given the fact that the (111) twinned silicon nanolayered structures can be prepared by molecular-beam epitaxy, the further experiments on uniaxial compression of such structures would be appropriate to verify our theoretical results.

ACKNOWLEDGMENTS

This work was supported by the STCU under Contract No. 4682. The work of P.T. was performed under the auspices of the U. S. Department of Energy by the Lawrence Livermore National Laboratory under Contract No. DE-AC52-07NA27344.

[1] J. Z. Hu, L. D. Merkle, C. S. Menoni, and I. L. Spain, Phys. Rev. B **34**, 4679 (1986).
[2] J. Z. Hu and I. L. Spain, Solid State Commun. **51**, 263 (1984).
[3] M. I. McMahon and R. J. Nelmes, Phys. Rev. B **47**, 8337 (1993).
[4] M. I. McMahon, R. J. Nelmes, N. G. Wright, and D. R. Allan, Phys. Rev. B **50**, 739 (1994).
[5] H. Olijnyk, S. K. Sikka, and W. B. Holzapfel, Phys. Lett. A **103**, 137 (1984).
[6] Y.-X. Zhao, F. Buehler, F. R. Sites, and I. L. Spain, Solid State Commun. **59**, 679 (1986).
[7] M. Imai, K. Yaoita, Y. Katayama, J.-Q. Chen, and K. Tsuji, J. Non-Cryst. Solids **150**, 49 (1992).
[8] R. Wentorf and J. Kasper, Science **139**, 338 (1963).
[9] J. Crain, G. J. Ackland, J. R. Maclean, R. O. Piltz, P. D. Hatton, and G. S. Pawley, Phys. Rev. B **50**, 13043 (1994).
[10] O. Shimomura, S. Minomura, N. Sakai, K. Asaumi, K. Tamuraand, J. Fukushima, and H. Endo, Philos. Mag. **29**, 547 (1974).
[11] H. Balamane, T. Halicioglu, and W. A. Tiller, Phys. Rev. B **46**, 2250 (1992).
[12] F. Zandiehnadem and W. Y. Ching, Phys. Rev. B **41**, 12162 (1990).
[13] K. Mizushima, S. Yip, and E. Kaxiras, Phys. Rev. B **50**, 14952 (1994).
[14] M. Bernasconi, G. L. Chiarotti, P. Focher, S. Scandolo, E. Tosatti, and M. Parrinello, J. Phys. Chem. Solids **56**, 501 (1995).
[15] T. Morishita and S. Nosè, RIKEN Rev. **29**, 94 (2000).
[16] C. Cheng, Phys. Rev. B **67**, 134109 (2003).
[17] P. Valentini, W. W. Gerberich, and T. Dumitrica, Phys. Rev. Lett. **99**, 175701 (2007).
[18] R. L. Headrick, B. E. Weir, J. Bevk, B. S. Freer, D. J. Eaglesham, and L. C. Feldman, Phys. Rev. Lett. **65**, 1128 (1990).
[19] H. Hibino and T. Ogino, Mater. Sci. Eng., B **87**, 214 (2001).
[20] A. Fissel, E. Bugiel, C. Wang, and H. Osten, J. Cryst. Growth **290**, 392 (2006).
[21] J. Tersoff, Phys. Rev. B **39**, 5566 (1989).
[22] http://xmd.sf.net, 2000.
[23] S. Baroni *et al.*, http://www.pwscf.org/, 2009.
[24] D. Vanderbilt, Phys. Rev. B **41**, 7892 (1990).
[25] J. P. Perdew, K. Burke, and M. Ernzerhof, Phys. Rev. Lett. **77**, 3865 (1996).
[26] H. J. Monkhorst and J. D. Pack, Phys. Rev. B **13**, 5188 (1976).
[27] M. Parrinello and A. Rahman, Phys. Rev. Lett. **45**, 1196 (1980).
[28] V. I. Ivashchenko, P. E. A. Turchi, V. I. Shevchenko, L. A. Ivashchenko, and O. A. Shramko, Phys. Rev. B **71**, 165209 (2005).
[29] H. T. Stokes, D. M. Hatch, and B. J. Campbell, ISOTROPY, http://stokes.byu.edu/isotropy.html, 2007.